Fuel 333 (2023) 126455

Contents lists available at ScienceDirect

Fuel

journal homepage: www.elsevier.com/locate/fuel

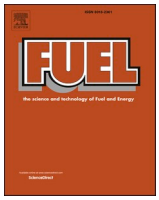

Full Length Article

Reactive force field molecular dynamics simulation of pyridine combustion assisted by an electric field

Zhongze Bai [a], Xi Zhuo Jiang [b,*], Kai H. Luo [a,*]

[a] Department of Mechanical Engineering, University College London, Torrington Place, London WC1E 7JE, UK
[b] School of Mechanical Engineering and Automation, Northeastern University, Shenyang, Liaoning 110819, China

ARTICLE INFO

Keywords:
Pyridine oxidation
Electric field
Reactive force field
Molecular dynamics

ABSTRACT

The reduction of nitrogen oxides (NOx) is a perennial challenge for fuel combustion. Electric field enhanced combustion is a promising technology to decrease NOx emissions during the combustion process. This study aims to investigate the effects of electric field on fuel-NOx formation during pyridine (the main nitrogen-containing compounds in fossil fuels) combustion. The yields of main products (NO, NO_2, N_2, CO and CO_2) are investigated during pyridine oxidation with external electric field imposed. Results indicate that electric field can reduce emissions (CO and NO) during pyridine combustion. Moreover, the reaction mechanisms of pyridine oxidation under different electric fields are explored at atomic scales, which provides an explanation for the changes of main products at varying electric field characteristics. This study fills the current knowledge gaps concerning the electric field influence on fuel-NOx emissions, which has the potential to form control strategies for NOx emissions during fossil fuel combustion.

1. Introduction

The reduction of nitrogen oxides (NOx) is a long-lasting challenge for fuel combustion. Electric field (EF) enhanced combustion is a promising technology to decrease NOx emissions by modifying the reaction mechanisms during combustion process [1–3]. To develop a control strategy of NOx emissions from combustion via EF, both qualitative and quantitative understanding of the effects of electric field on fuel combustion is of great importance.

There have been many efforts to reveal the EF effects on NOx formation during fuel combustion. For instance, Zake and co-workers carried out experiments to investigate the EF influence on NO emissions during natural gas combustion [4]. They proposed that EF could decrease thermal NOx formation up to 30–80 % during natural gas combustion [4]. An experimental study of EF influence on biomass gasifier combustion was conducted by Barmina and co-workers [5]. Results indicated that CO and NOx emissions were reduced when external EF was applied. Most and co-workers found that EF could control NOx emissions during methane combustion in air [6]. Previous studies by experiments and CFD simulations also demonstrated that EF could reduce NO_X emissions during propane combustion in air [7–9]. Though the above findings demonstrate the overall effects of EF on NO emissions during fuel combustion, many questions remain. For example, except thermal NOx, could the electric field control fuel-NOx formation? How would the EF strength affect the NOx emissions quantitatively? To resolve those questions, more detailed studies using time- and space-resolved methods are desired. Another observation is that previous studies on this topic have employed simple gaseous fuels, while more complex fuels or solid fuels have not been investigated.

Due to the limitations of current measurement techniques, experimental studies cannot provide time-resolved, full-field information, making it hard to accurately reveal the underlying chemical mechanisms during fuel combustion. Alternatively, a high-resolution computational method called Reactive Force Field Molecular Dynamics (ReaxFF MD) can overcome this problem by revealing reaction mechanisms at the atomic level with acceptable computational cost. ReaxFF MD simulations have recently been applied to investigate mechanisms for the EF effects on ethanol [10,11], hydrogen/methane [12], toluene [13], *n*-dodecane [14] combustion as well as *n*-decane [15] and RDX molecular crystals [16] pyrolysis. The aim of the present study is to extend the investigation to more complex fossil fuels. As the molecular structures of fossil fuels are complex and uncertain [17], pyridine, the main nitrogen-containing compounds in fossil fuels [18–20], is used as a surrogate for the source of fuel-NOx emissions.

* Corresponding authors.
E-mail addresses: jiangxz@mail.neu.edu.cn (X.Z. Jiang), k.luo@ucl.ac.uk (K.H. Luo).

https://doi.org/10.1016/j.fuel.2022.126455
Received 28 July 2022; Received in revised form 4 October 2022; Accepted 19 October 2022
Available online 29 October 2022

Table 1
Initial parameters of studied systems.

System	Number of C_5H_5N molecules	Number of O_2 molecules	E/V·nm^{-1}	Density (g/cm^3)	Box size (nm)
1	80	540	0	0.3	5.07
2	80	540	1	0.3	5.07
3	80	540	2.5	0.3	5.07
4	80	540	5	0.3	5.07
5	80	540	7.5	0.3	5.07

In this study, we performed ReaxFF simulations to investigate the effects of EF on pyridine combustion. The main objectives of this paper are: (a) to study the EF influence on the yields of main products (CO, CO_2, NO, NO_2 and N_2); (b) to identify the formation mechanisms of main products under varying electric field strengths; (c) to explain the effects of EF on the generation of key products from the atomic perspective.

2. Methods

2.1. ReaxFF MD

The ReaxFF is a force field method that was originally developed by van Duin and co-workers [21]. ReaxFF employs a bond-order formalism in conjunction with polarizable charge descriptions to determine both reactive and non-reactive interactions between atoms [22]. Energy contributions to the ReaxFF potential are shown as follows:

$$E_{system} = E_{bond} + E_{over} + E_{angle} + E_{tors} + E_{vdWaals} + E_{Coulomb} + E_{Specific} \quad (1)$$

where the terms are total energy, bond energy, penalty energy, valence angle energy, torsion angle energy, van der Waals energy, Coulomb energy and specific energy, respectively [22].

2.2. Case set-ups

The initial parameters of studied systems are shown in Table 1. The number of pyridine molecules in every system is 80 and the density is 0.3 g/cm^3. The equivalence ratio (λ) of pyridine oxidation is calculated based on the following global reaction:

$$C_5H_5N + 6.75O_2 \rightarrow 5CO_2 + NO + 2.5H_2O \quad (2)$$

System 1 simulates pyridine oxidation in air under stoichiometric conditions ($\lambda = 1$). In systems 2 ~ 5, to study the effects of EF on pyridine combustion, electric strengths ranging from 1 ~ 7.5 V/nm are imposed in the +x direction. The details of system configurations are shown in Fig. 1.

2.3. Simulation details

Large-scale Atomic/Molecular Massively Parallel Simulator (Lammps) [23,24] and the reactive force field of C/H/O/N parameters [25,26] were used for all ReaxFF MD simulations. The time step and cutoff values were chosen to be 0.1 fs and 0.3, respectively. The canonical ensemble (NVT) [27] was selected for all ReaxFF MD simulations. Firstly, every system underwent energy minimization and system equilibration at a temperature of 500 K for 100 ps. Afterwards, the system temperature was raised to the final temperature at 2600 K with a heating rate of 100 K/ps. Then the system temperature was kept constant. The total simulation time was 1000 ps. All output information was recorded every 100 fs. To avoid biases during the simulation process, all simulations were performed three times.

2.4. Post-processing

The visualisations of atomic trajectories were produced using the VMD software [28]. Chemical Trajectory Analyzer (ChemTrayzer) scripts was used to analyse reaction pathways [29]. The data used in the figures are the average results of three replicate simulations for each case. Error bars in all figures are Standard Error (SE) of three replicates. The net flux (NF) was calculated for every individual reaction, which means the number of times the direct reaction occurred minus the number of times the reverse reaction happened [30].

3. Results

3.1. Time evolution of reactants and species number

The time evolutions of C_5H_5N and O_2 with EF strengths ranging from 0 to 7.5 V/nm are used to study the influence of EF on reaction rates of reactants during the combustion process. As shown in Fig. 2a and 2b, EF inhibits the consumption of C_5H_5N and O_2 in $E = 0$–2.5 V/nm, however, accelerates reaction rates with EF strength of 2.5–7.5 V/nm. Fig. 2c and 2d show the number of species in systems under varying EF strengths as

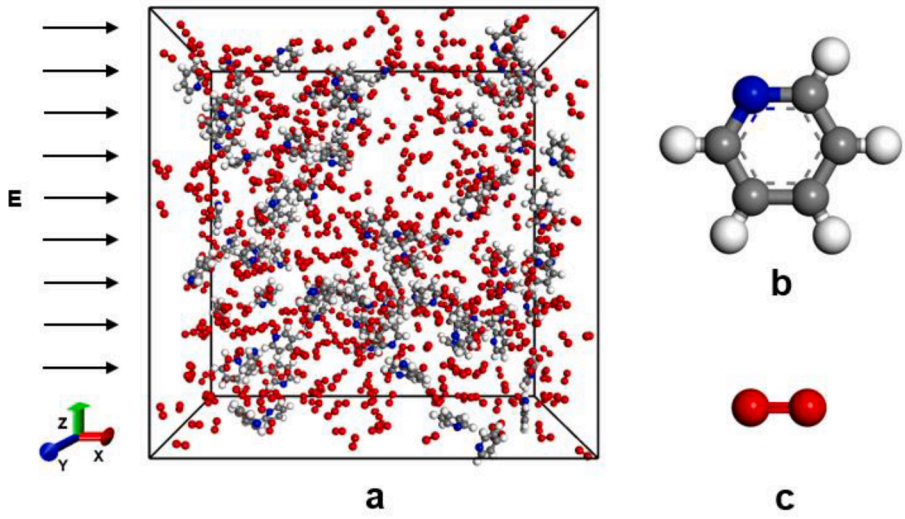

Fig. 1. System configurations for pyridine oxidation under varying EF strength. (a) pyridine oxidation system, (b) pyridine structure, (c) O_2 structure. C, H, O and N atoms are represented in grey, white, red and blue, respectively. (For interpretation of the references to colour in this figure legend, the reader is referred to the web version of this article.)

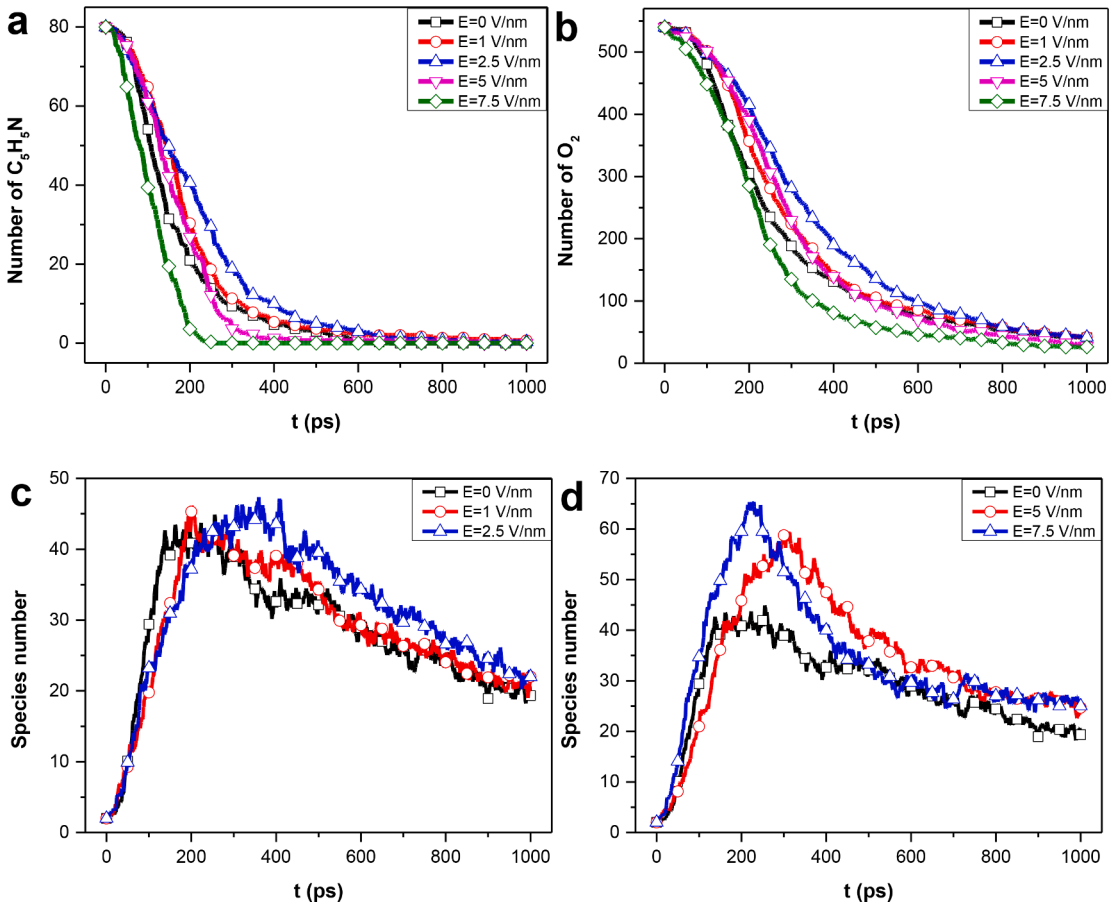

Fig. 2. Time evolution of reactants and species number. (a) C_5H_5N; (b) O_2; (c) species number (E = 0 ~ 2.5 V/nm); (d) species number (E = 0&5&7.5 V/nm).

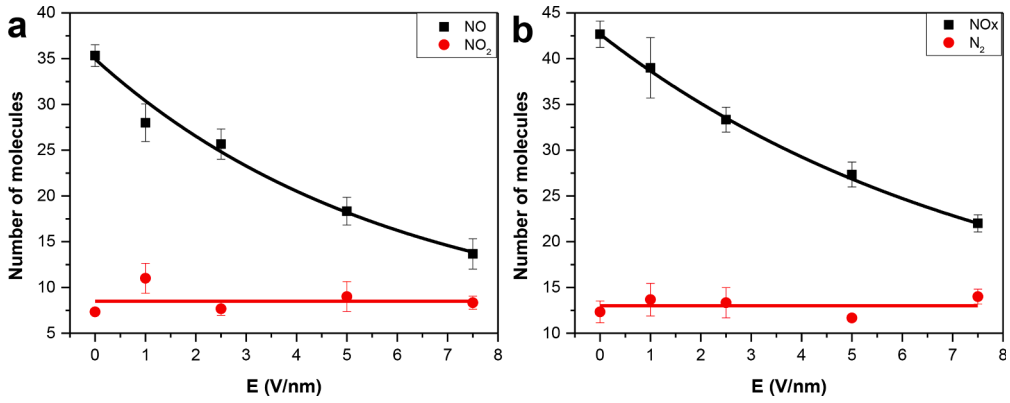

Fig. 3. Effects of EF on the yield of main nitrogen-containing products. (a) NO and NO_2; (b) NOx (NO + NO_2) and N_2.

the reaction goes. Overall, the number of species first increases to the peak point promptly and then decreases subsequently in all cases. Besides, the maximum species number formed during pyridine combustion rises as EF strength increases. The above findings imply that the imposition of EF modifies the reaction rates of reactants and the formation of species during pyridine oxidation, which agrees with previous studies [10,11].

3.2. Effects of electric field on nitrogen-containing products (NO, NO_2 and N_2)

Fig. 3 shows the effects of the EF on the generation of key nitrogen-containing products. As the EF strength increases, the yield of NO shows a downward trend when the E value is in the range of 0–7.5 V/nm. However, EF has an insignificant influence on the generation of NO_2 and N_2 at the end of simulations in all cases. In addition, as NO dominates over NO_2 in magnitude, the trend of NOx (the sum of NO and NO_2) variations with respect to EF is the same with that of NO.

To reveal how the EF changes the generation of key products, transfer pathways of main nitrogen-containing intermediates with and without the imposition of EF were scrutinized and compared. Generally, pyridine molecules are oxygenated to oxygen-containing intermediates (C_5H_5NO, $C_5H_4NO_2$, C_5H_4NO and $C_5H_3NO_2$) first. Then those intermediates open rings to form chain species. After that, the chain decomposes into HCN, CN, CNO and HNO, which will convert to main nitrogen-containing products via a series of reactions. The findings on

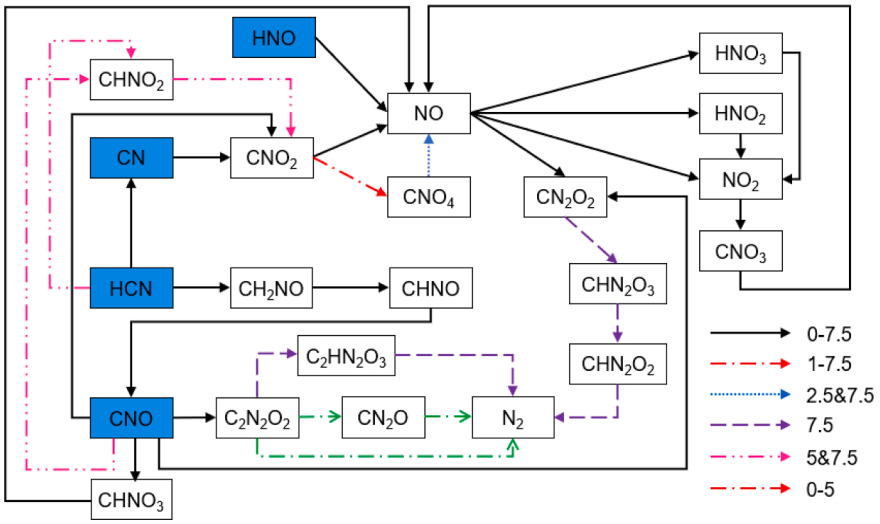

Fig. 4. Effects of EF on transfer pathways of main nitrogen-containing intermediates. The radicals in the blue box are the starting intermediates. The numerical values in the figure are intensities of electric field. (For interpretation of the references to colour in this figure legend, the reader is referred to the web version of this article.)

Table 2
Net flux (NF) of reaction pathways linked with NO, NO_2 and N_2 in $E = 0 \sim 7.5$ V/nm.

Pathways	0	1	2.5	5	7.5
$CNO_2 \rightarrow NO$	90	86	55	56	33
$HNO \rightarrow NO$	13	7	13	7	−1
$CHNO_3 \rightarrow NO$	14	5	9	22	18
$CNO_3 \rightarrow NO$	12	12	5	8	10
$CNO_4 \rightarrow NO$	0	0	11	0	2
Total NO generation	129	110	93	93	62
$NO \rightarrow CN_2O_2$	8	6	13	14	19
$NO \rightarrow NO_2$	3	4	4	9	−5
$NO \rightarrow HNO_3$	17	7	8	2	13
$NO \rightarrow HNO_2$	2	23	14	33	32
NO consumption	30	40	39	58	59
Net NO generation	99	70	54	35	3
$NO \rightarrow NO_2$	3	4	4	9	−5
$HNO_3 \rightarrow NO_2$	13	5	2	−3	2
$HNO_2 \rightarrow NO_2$	1	17	5	13	12
Total NO_2 generation	17	26	11	19	9
$NO_2 \rightarrow CNO_3$	7	11	4	2	1
Net NO_2 generation	10	15	7	17	8
$CN_2O \rightarrow N_2$	5	10	8	7	0
$C_2N_2O_2 \rightarrow N_2$	7	8	8	3	0
$CHN_2O_2 \rightarrow N_2$	0	0	0	0	7
$C_2HN_2O_3 \rightarrow N_2$	0	0	0	0	6
Total N_2 generation	12	18	16	10	13

the reaction mechanisms of pyridine oxidation are in good agreement with previous results [31]. Here, we focused on the influence of the EF on the reaction pathways from HCN, CN, CNO and HNO to key nitrogen-containing products (NO, NO_2 and N_2).

As shown in Fig. 4, $C_2N_2O_2$ is an important intermediate for N_2 generation, which is formed by reaction R1 ($CNO + CNO \rightarrow C_2N_2O_2$) in all cases. The pathways $C_2N_2O_2 \rightarrow CN_2O \rightarrow N_2$ and $C_2N_2O_2 \rightarrow N_2$ by reactions R2 ($C_2N_2O_2 \rightarrow CN_2O + CO$) and *R*3 ($CN_2O \rightarrow N_2 + CO$) and R4 ($C_2N_2O_2 \rightarrow N_2 + 2CO$) occur in $E = 0$–5 V/nm cases. However, when the EF strength is 7.5 V/nm, N_2 is generated through pathways $C_2N_2O_2 \rightarrow C_2HN_2O_3 \rightarrow N_2$ and $CN_2O_2 \rightarrow CHN_2O_3 \rightarrow CHN_2O_2 \rightarrow N_2$. Five pathways for forming NO are determined during pyridine combustion. In all conditions, NO is generated by thermal decomposition of CNO_2, $CHNO_3$ as well as CNO_3 and HNO oxidation reactions with O_2, OH and HO_2. The pathway $CNO_2 \rightarrow CNO_4 \rightarrow NO$ is found in $E = 2.5$ and 7.5 V/nm conditions. NO molecules are consumed by the generation of HNO_2, HNO_3, NO_2 and CN_2O_2 in both electric and electric-free conditions. The formation of NO_2 is via pathways $NO \rightarrow HNO_2 \rightarrow NO_2$, $NO \rightarrow HNO_3 \rightarrow NO_2$ and $NO \rightarrow NO_2$ in all conditions. The conversion from NO_2 to CNO_3 is the only pathway for NO_2 consumption. The pathway of $CNO/HCN \rightarrow CHNO_2 \rightarrow CNO_2$ is observed in $E = 5$ and 7.5 V/nm cases.

To further identify the contributions of each pathway to the formation of NO, NO_2 and N_2, the net flux (NF) analysis of key reaction pathways is summarised in Table 2. Overall, the net NF and yields of main products (NO, NO_2 and N_2) changes with the EF strength, which proves the effectiveness of the NF analysis in detailed investigation of the underlying mechanisms.

Specifically, the increase of EF strength inhibits NO generation, by contrast, promotes NO consumption during pyridine combustion. Among them, the influence of EF on the contributions of CNO_2 and CNO_3 to the formation of NO is not significant. However, the NF of $CNO_2 \rightarrow NO$ via R5 ($CNO_2 \rightarrow CO + NO$) decreases with EF strength, which accounts for the changes of total NO generation under varying conditions. As for NO consumption, EF promotes the conversion from NO to CN_2O_2 and HNO_2, however, presents unsignificant influence on the pathways $NO \rightarrow NO_2$ and $NO \rightarrow HNO_3$. Thereby, the promotion of NO consumption with increasing EF strength is mainly through pathways $NO \rightarrow CN_2O_2$ via R6 ($NO + CNO \rightarrow CN_2O_2$) and $NO \rightarrow HNO_2$ via R7 ($NO + OH \rightarrow HNO_2$).

Regarding NO_2, the effects of EF on NO_2 generation and consumption ($NO_2 \rightarrow CNO_3$) are almost the same over $E = 0$–7.5 V/nm. When the value of EF strength is in the range of 0 to 1 V/nm, the NO_2 generation and consumption increase with increasing EF strength, whereas the increasing EF strength leads to a decrease of the conversion when E is greater than 1 V/nm. Those results suggest that the insignificant influence of EF on net NF of NO_2 generation is the collective contribution of both NO_2 formation and consumption. The NO_2 formation from HNO_3 by reactions R8 ($HNO_3 \rightarrow NO_2 + OH$) and R9 ($HNO_3 + OH \rightarrow H_2O_2 + NO_2$) is weakened as *E* increases. The conversion from HNO_2 to NO_2 is enhanced by the increase of EF strength over E = 0–1 V/nm. Conversely, the increasing EF strength slightly inhibits the NO_2 formation when E is in the range of 1 to 7.5 V/nm. Therefore, the influence of EF on NO_2 generation is through the co-contribution of HNO_3 and HNO_2 to NO_2 with EF strength increasing. Though the EF changes the reaction pathways of N_2 formation from CN_2O (R3) and $C_2N_2O_2$ (R4) to CHN_2O_2 via R10 ($CHN_2O_2 \rightarrow N_2 + CHO_2$) and $C_2HN_2O_3$ via R11 ($C_2HN_2O_3 \rightarrow N_2 + CHO_2 + CO$) in the $E = 7.5$ V/nm case, the total NF of N_2 generation almost remains the same under various EF strengths.

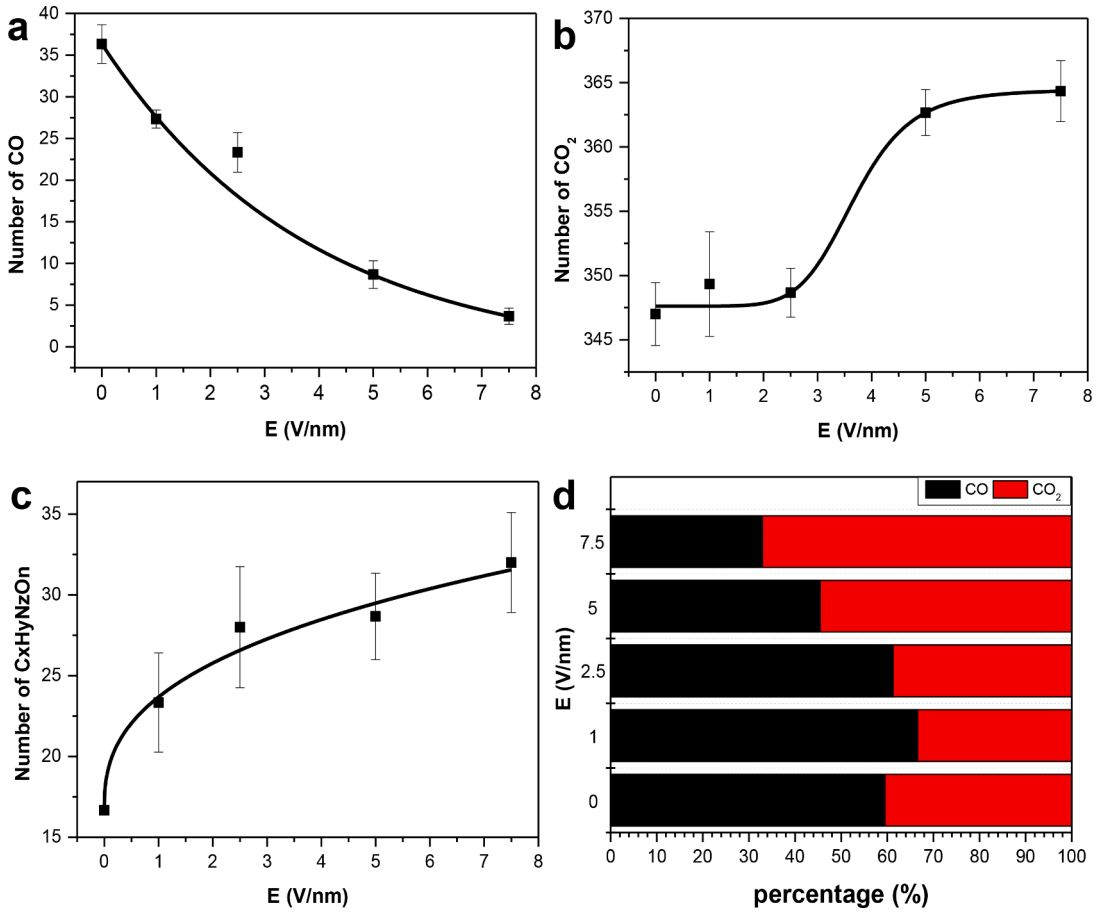

Fig. 5. Effects of EF on main nitrogen-free products. (a) CO; (b) CO_2; (c) unburn carbons (CxHyNzOn); (d) proportion of CO and CO_2 generated by thermal decomposition of oxygen-containing intermediates.

Table 3
Net flux (NF) of reaction pathways related to CO and CO_2 in $E = 0 \sim 7.5$ V/nm.

Pathways	0	1	2.5	5	7.5
$CO \rightarrow CO_2$	171	159	142	69	26
$CO \rightarrow CO_3$	259	258	236	213	205
$CO \rightarrow CHO_2$	126	84	84	47	26
$CO \rightarrow CHO_3$	21	21	30	10	10
Total CO consumption	577	522	492	339	267
$CO \rightarrow CO_2$	171	159	142	69	26
$CO_3 \rightarrow CO_2$	163	182	165	138	125
$CHO_2 \rightarrow CO_2$	101	115	127	147	97
$CHO_3 \rightarrow CO_2$	65	66	85	80	116
$CHO_4 \rightarrow CO_2$	10	0	16	26	27
$CO_4 \rightarrow CO_2$	0	0	0	7	20
Total CO_2 generation	510	522	535	467	411

3.3. Effects of electric field on carbon-containing products (CO and CO_2)

Fig. 5a-5c compare the yields of CO, CO_2 and unburned carbon (CxHyNzOn) at varying EF conditions. As the EF strength increases, the generation of CO is inhibited over $E = 0$–7.5 V/nm. However, as the EF increases, the number of CO_2 keeps the same firstly with E raging from 0 to 2.5 V/nm, while shows an upward trend over $E = 2.5$–7.5 V/nm. The increase of EF also promotes the yield of unburned carbon (CxHyNzOn) at the end of simulations. To illustrate how the EF affects the yields of CO and CO_2, we explored the reaction mechanisms of CO and CO_2 at varying electric strengths during pyridine oxidation.

During pyridine combustion, two stages are observed for CO and CO_2 generation. Firstly, pyridine molecules are oxygenated to oxygen-containing intermediates, followed by ring-opening reactions forming chain species. Those chained intermediates undergo thermal decomposition forming CO and CO_2 by reactions R12 ($C_xH_yN_zO_n \rightarrow C_{x\text{-}1}H_yN_zO_{n\text{-}2} + CO_2$) and R13 ($C_xH_yN_zO_n \rightarrow C_{x\text{-}1}H_yN_zO_{n\text{-}1} + CO$). As observed in Fig. 5d, EF slightly inhibits the generation of CO_2 generated from decomposition of oxygen-containing intermediates in E = 1 and 2.5 V/nm cases. However, when the value of EF strength is larger than 2.5, R12 is significantly enhanced by the increase of E values. After that, there is CO_2 formation through the conversion from CO to CO_2. The NF of pathways related to CO and CO_2 under different electric field intensities is listed in Table 3.

For CO consumption, four pathways were observed, which are $CO \rightarrow CO_2$, $CO \rightarrow CO_3$, $CO \rightarrow CHO_2$ and $CO \rightarrow CHO_3$. EF shows strong inhibition effects, in terms of NF, on the conversion from CO to CO_2, CO_3 and CHO_2 mainly through the following reactions:

$$CO + HO_2 \rightarrow CO_2 + OH \quad (R14)$$

$$CO + O_2 \rightarrow CO_2 + O \quad (R15)$$

$$CO + NO_2 \rightarrow CO_2 + NO \quad (R16)$$

$$CO + O_2 + HO \rightarrow CO_2 + HO_2 \quad (R17)$$

$$CO + O \rightarrow CO_2 \quad (R18)$$

$$CO + HO \rightarrow CO_2 + H \quad (R19)$$

$$CO + O2 \rightarrow CO_3 \quad (R20)$$

$$CO + HO \rightarrow CHO_2 \quad (R21)$$

$$CO + H_2O_2 \rightarrow CHO_2 + HO \quad (R22)$$

And the NF of CO → CHO_3 via R23 (CO + HO_2 → CHO_3) is less affected by changes in EF strength. The NF of total NO consumption shows a downward trend with EF intensities. As mentioned previously, EF promotes the unburned carbon formation in all cases, and decreases the CO_2 generated from decomposition of oxygen-containing intermediates in E = 5 and 7.5 V/nm cases. Thus, the decrease of CO number with EF intensities is main caused by the inhibition effects of CO generation during pyridine combustion.

Table 3 also indicates that CO, CO_3, CHO_2, CHO_3, CHO_4 and CO_4 are key precursors for CO_2 generation. Specifically, the conversion from CO to CO_2 by reactions R15-R19 is enhanced by EF strength in all conditions. Besides, as EF intensities increase, the NF of CO_3 → CO_2 shows a parabolic trend and reaches the peak point at E = 1 V/nm mainly by R23 (CO_3 → CO_2 + O). The conversion from CHO_2 to CO_2 is enhanced by EF in E = 0–5 V/nm cases, but decreases with E ranging from 5 to 7 V/nm. Reaction R24 (CHO_2 + O_2 → CO_2 + HO_2) plays a vital role on the conversion of CHO_2 to CO_2 under varying conditions. High EF also promotes CO_2 generation from CHO_3 via R25 (CHO_3 → CO_2 + HO) and CO_4 via R26 (CO_4 → CO_2 + O_2). The NF of pathway CHO_4 → CO_2 through R27 (CHO_4 → CO_2 + HO_2) first decreases with E = 0–1 V/nm, and then increases when EF strength is larger than 1 V/nm. Overall, the total NF of CO_2 formation is slightly enhanced over E = 0–2.5 V/nm, but decreases with E ranging from 2.5 to 7.5 V/nm. While the CO_2 from the decomposition of oxygen-containing intermediates in E = 1–2.5 V/nm cases, the promotional influence of EF on CO_2 production causes the yield of CO_2 to almost remain constant. When E is larger than 2.5 V/nm, the reaction R12 plays a domain position on CO_2 generation, causing the increase of CO_2 yield at the end of simulations.

4. Discussion

In the present study, we shed light on the effects of EF on pyridine oxidation through ReaxFF MD simulations for the first time. Results indicate that EF plays a positive role in the control of formation of emissions (NO and CO) during fuel combustion. Furthermore, the changes of main products (NO, NO_2, N_2, CO and CO_2) are interpreted at the atomic scale.

The EF can modify reaction pathways during fuel combustion by making charge carriers move in specified directions, thus altering the interactions between charged intermediates [32]. Besides, the collision of accelerated particles with neutral molecules increases the reactivity of the mixture. As a result, the reaction mechanisms are modified by EF during the combustion process.

The performance of EF in controlling emissions under different electric intensities is compared as well. According to the above analysis, the inhibition influence of EF on emissions is outstanding at E = 7.5 V/nm, where the yields of NO, NOx and CO are reduced by 61 %, 48 % and 90 %, respectively. Meanwhile, the increase of EF strength also promotes the unburned hydrocarbons, leading to the decrease of combustion efficiency and increase of the ash formation. Thus, by varying the intensities of the EF, different requirements for emissions can be achieved.

EF intensities required in ReaxFF MD simulations are usually several orders of magnitude larger than those in experiments because of a temporal difference between experimental and simulation timescales, which is also supported by previous studies [33–35]. ReaxFF MD often uses greater temperatures than in experiments to speed simulations because of the high computational cost, which has been validated to reproduce reaction mechanisms observed in experiments [36–38]. Under this strategy, the random motion of particles is significantly faster than that in experiments. Therefore, more strong EF intensities are required to change the motion of particles and final yields of products in MD simulations.

5. Conclusions

In this study, ReaxFF MD simulations were conducted to investigate the effects of EF on pyridine combustion. The consumption rates of reactants and yields of main products (NO, NO_2, N_2, CO and CO_2) are influenced during pyridine oxidation by imposed external EF. Besides, the reaction mechanisms of pyridine oxidation under different EF strengths are explored at atomic scales, which can explain the changes in the yields of main products at varying EF strengths. Results indicate that EF suppresses C_5H_5N and O_2 consumption at E = 0–2.5 V/nm but enhances the reaction rates at E = 2.5–7.5 V/nm. And the maximum number of species generated during pyridine combustion grows as the EF strength increases. In addition, EF decreases the yields of NO and CO, however, shows an insignificant influence on NO_2 and N_2 in all cases. The yield of CO_2 almost remains constant at E = 0–2.5 V/nm, but increases when EF strength is larger than 2.5 V/nm via reaction $C_xH_yN_zO_n$ → $C_{x-1}H_yN_zO_{n-2}$ + CO_2. In particular, EF inhibits the formation of NO by pathway CNO_2 → NO (CNO_2 → CO + NO), however promotes NO consumption through pathways NO → CN_2O_2 (NO + CNO → CN_2O_2) and NO → HNO_2 (NO + OH → HNO_2). This study fills a knowledge gap regarding the EF influence on fuel-NOx emissions, which facilitates the development of strategies for controlling NOx emissions during fossil fuel combustion.

Table A1
Full list of elementary reactions during pyridine combustion.

CNO_2 → NO	**CNO_4 → NO**
CNO_2 → CO + NO	CNO_4 → CO_3 + NO
O_2 + CNO_2 → CO_3 + NO	**CHN_2O_2 → N2**
HNO → NO	CHN_2O_2 → N_2 + CHO_2
HNO + HO → H_2O + NO	**$C_2HN_2O_3$ → N_2**
HNO + HO_2 → H_2O_2 + NO	$C_2HN_2O_3$ → N_2 + CHO_2 + CO
H + NO → HNO	**CO → CO_2**
HNO + O → NO + HO	CO + HO_2 → CO_2 + HO
HNO + O_2 → HO_2 + NO	CO + O_2 → CO_2 + O
$CHNO_3$ → NO	CO + NO_2 → CO_2 + NO
$CHNO_3$ → CHO_2 + NO	CO + O_2 + HO → CO_2 + HO_2
CNO_3 → NO	CO + O → CO_2
CNO_3 → CO_2 + NO	CO + HO → CO_2 + H
NO → CN_2O_2	CO + H_2O_2 → H_2O + CO2
CNO + NO → CN_2O_2	**CO → CO_3**
NO → NO_2	CO + O_2 → CO_3
CO + NO_2 → CO_2 + NO	**CO → CHO_2**
HO2 + NO → HO + NO_2	CO + HO → CHO_2
H_2O_2 + NO → H_2O + NO_2	CO + H_2O_2 → CHO_2 + HO
NO + O → NO_2	CO + HO_3 → O_2 + CHO_2
H + NO_2 → NO + HO	**CO → CHO_3**
NO → HNO_3	CO + HO_2 → CHO_3
HO_2 + NO → HNO_3	**CO_3 → CO_2**
NO → HNO_2	CO_3 → CO_2 + O
H_2O_2 + NO → HNO_2 + HO	CO_3 + H_2O → CO_2 + HO + HO
NO + HO → HNO_2	H_2O + CO_3 → CO_2 + H_2O_2
HNO_2 + CO → CHO_2 + NO	CO_3 + HO → CO_2 + HO_2
HNO_3 → NO_2	CO + CO_3 → CO_2 + CO_2
HNO_3 → HO + NO_2	CO_3 + O_2 → CO_2 + O_3
HNO_3 + HO → H_2O_2 + NO_2	CO_3 + HO_2 → CO_2 + O_2 + HO
HNO_2 → NO_2	**CHO_2 → CO_2**
HNO_2 + HO → H_2O + NO_2	CHO_2 + O_2 → CO_2 + HO_2
O_2 + HNO_2 → HO_2 + NO_2	CHO_2 → CO_2 + H
HNO_2 + O → HO + NO_2	CHO_2 + HO → H_2O + CO_2
H + NO_2 → HNO_2	CHO_2 + HO_2 → CO_2 + H_2O_2
HNO_2 + HO_2 → H_2O_2 + NO_2	CHO_2 + H_2O_2 → H_2O + CO_2 + HO
NO_2 → CNO_3	**CHO_3 → CO_2**
CO + NO_2 → CNO_3	CHO_3 → CO_2 + HO
CN_2O → N_2	O_2 + CHO_3 → CO_2 + HO_3
CN_2O → N_2 + CO	**CHO_4 → CO_2**
$C2N_2O_2$ → N_2	CHO_4 → CO_2 + HO_2
$C_2N_2O_2$ → N_2 + CO + CO	**CO_4 → CO_2**
	CO_4 → CO2 + O_2

CRediT authorship contribution statement

Zhongze Bai: Conceptualization, Methodology, Software, Investigation, Data curation, Visualization, Writing – original draft. **Xi Zhuo Jiang:** Supervision, Writing – review & editing. **Kai H. Luo:**

Supervision, Funding acquisition, Resources, Project administration, Writing – review & editing.

Declaration of Competing Interest

The authors declare that they have no known competing financial interests or personal relationships that could have appeared to influence the work reported in this paper.

Data availability

Data will be made available on request.

Acknowledgements

Support from the UK Engineering and Physical Sciences Research Council under the grant No. EP/S012559/1 is gratefully acknowledged. The supercomputing time is provided by the "UK Consortium on Mesoscale Engineering Sciences (UKCOMES)" (Grant No. EP/R029598/1). This work made use of computational support by CoSeC, the Computational Science Centre for Research Communities, through UKCOMES.

Appendix A

See

References

[1] Imamura O, Chen B, Nishida S, Yamashita K, Tsue M, Kono M. Combustion of ethanol fuel droplet in vertical direct current electric field. Proc Combust Inst 2011;33(2):2005–11.
[2] Bradley D, Nasser S. Electrical coronas and burner flame stability. Combust Flame 1984;55(1):53–8.
[3] Altendorfner F, Kuhl J, Zigan L, Leipertz A. Study of the influence of electric fields on flames using planar LIF and PIV techniques. Proc Combust Inst 2011;33(2):3195–201.
[4] Zake M, Turlajs D, Purmals M. Electric field control of NOx formation in the flame channel flows. Global Nest: The Int J 2000;2(1):99–108.
[5] Barmina I, Kolmickovs A, Valdmanis R, Zake M. Control of combustion dynamics by an electric field. Chem Eng Trans 2015;43:973–8.
[6] Most D, Hammer T, Lins G, Branston D, Altendorfner F, Beyrau F, et al., editors. Electric Field Effects for Combustion Control-Optimized Geometry. International Conference on Phenomena in Ionized Gases; 2007.
[7] Vatazhin A, Likhter V, Sepp V, Shul'Gin V. Effect of an electric field on the nitrogen oxide emission and structure of a laminar propane diffusion flame. Fluid Dyn 1995;30(2):166–74.
[8] Krickis O, Jaundālders S, editors. Impact of electric field in the stabilized premixed flame on NOx and CO emissions. 2017 IEEE 58th International Scientific Conference on Power and Electrical Engineering of Riga Technical University (RTUCON); 2017: IEEE.
[9] Barmina I, Turlajs D, Zake M. Electric field effects on the swirling combustion dynamics. Rigas Tehniskas Universitates Zinatniskie Raksti 2008;1:39.
[10] Jiang XZ, Feng M, Zeng W, Luo KH. Study of mechanisms for electric field effects on ethanol oxidation via reactive force field molecular dynamics. Proc Combust Inst 2019;37(4):5525–35.
[11] Jiang XZ, Luo KH. Reactive and electron force field molecular dynamics simulations of electric field assisted ethanol oxidation reactions. Proc Combust Inst 2021;38(4):6605–13.
[12] Sun F, Zeng W. Electric field effects on hydrogen/methane oxidation: A reactive force field based molecular dynamics study. Int J Hydrogen Energy 2020;45(39):20194–9.
[13] Tan S, Xia T, Shi Y, Pfaendtner J, Zhao S, He Y. Enhancing the oxidation of toluene with external electric fields: a reactive molecular dynamics study. Sci Rep 2017;7(1):1–11.
[14] Kritikos E, Lele A, van Duin ACT, Giusti A. A reactive molecular dynamics study of the effects of an electric field on n-dodecane combustion. Combust Flame 2022;244:112238.
[15] Zhou W, Zhang X, Zhou W, Yang L, Jia Z. Inhibition mechanism of electric field on polycyclic aromatic hydrocarbon formation during n-decane pyrolysis: A ReaxFF MD and DFT study. J Energy Inst 2022;102:82–91.
[16] Miao F, Cheng X. Effect of electric field on polarization and decomposition of RDX molecular crystals: a ReaxFF molecular dynamics study. J Mol Model 2020;26(1):1–7.
[17] Wang C, Du Y, Jin Xi, Che D. Pyridine and pyrrole oxidation under oxy-fuel conditions. Energy Sources Part A 2016;38(7):975–81.
[18] Solomon PR, Colket MB. Evolution of fuel nitrogen in coal devolatilization. Fuel 1978;57(12):749–55.
[19] Nelson PF, Kelly MD, Wornat MJ. Conversion of fuel nitrogen in coal volatiles to NOx precursors under rapid heating conditions. Fuel 1991;70(3):403–7.
[20] Prado GH, Rao Y, de Klerk A. Nitrogen removal from oil: a review. Energy Fuels 2017;31(1):14–36.
[21] Van Duin AC, Dasgupta S, Lorant F, Goddard WA. ReaxFF: a reactive force field for hydrocarbons. J Phys Chem A 2001;105(41):9396–409.
[22] Senftle TP, Hong S, Islam MM, Kylasa SB, Zheng Y, Shin YK, et al. The ReaxFF reactive force-field: development, applications and future directions. NPJ Comput Mater 2016;2(1).
[23] Aktulga HM, Fogarty JC, Pandit SA, Grama AY. Parallel reactive molecular dynamics: Numerical methods and algorithmic techniques. Parallel Comput 2012;38(4–5):245–59.
[24] Plimpton S. Fast parallel algorithms for short-range molecular dynamics. J Comput Phys 1995;117(1):1–19.
[25] Zhang L, Duin ACTV, Zybin SV, Goddard III WA. Thermal decomposition of hydrazines from reactive dynamics using the ReaxFF reactive force field. J Phys Chem B 2009;113(31):10770–8.
[26] Zhang L, Zybin SV, Van Duin AC, Dasgupta S, Goddard III WA, Kober EM. Carbon cluster formation during thermal decomposition of octahydro-1, 3, 5, 7-tetranitro-1, 3, 5, 7-tetrazocine and 1, 3, 5-triamino-2, 4, 6-trinitrobenzene high explosives from ReaxFF reactive molecular dynamics simulations. J Phys Chem A 2009;113(40):10619–40.
[27] Andersen HC. Molecular dynamics simulations at constant pressure and/or temperature. J Chem Phys 1980;72(4):2384–93.
[28] Humphrey W, Dalke A, Schulten K. VMD: visual molecular dynamics. J Mol Graph 1996;14(1):33–8.
[29] Döntgen M, Przybylski-Freund M-D, Kröger LC, Kopp WA, Ismail AE, Leonhard K. Automated discovery of reaction pathways, rate constants, and transition states using reactive molecular dynamics simulations. J Chem Theory Comput 2015;11(6):2517–24.
[30] Arvelos S, Hori CE. ReaxFF study of ethanol oxidation in O_2/N_2 and O_2/CO_2 Environments at high temperatures. J Chem Inf Model 2020;60(2):700–13.
[31] Luo J, Zou C, He Y, Jing H, Cheng S. The characteristics and mechanism of NO formation during pyridine oxidation in O_2/N_2 and O_2/CO_2 atmospheres. Energy 2019;187:115954.
[32] Ma Y, Li T, Yan J, Wang X, Gao J, Sun Z. A comprehensive review of the influence of electric field on flame characteristics. 2020.
[33] English NJ, Waldron CJ. Perspectives on external electric fields in molecular simulation: progress, prospects and challenges. PCCP 2015;17(19):12407–40.
[34] English NJ, MacElroy J. Hydrogen bonding and molecular mobility in liquid water in external electromagnetic fields. J Chem Phys 2003;119(22):11806–13.
[35] Saitta AM, Saija F, Giaquinta PV. Ab initio molecular dynamics study of dissociation of water under an electric field. Phys Rev Lett 2012;108(20):207801.
[36] Wang J, Jiang XZ, Luo KH. Exploring reaction mechanism for ammonia/methane combustion via reactive molecular dynamics simulations. Fuel 2023;331:125806.
[37] Bai Z, Jiang XZ, Luo KH. Effects of water on pyridine pyrolysis: A reactive force field molecular dynamics study. Energy 2022;238:121798.
[38] Bai Z, Jiang XZ, Luo KH. A reactive molecular dynamics study of NO removal by nitrogen-containing species in coal pyrolysis gas. Proc Combust Inst 2022.